doi:10.1093/brain/awu256 Brain 2014: 137; 3036–3046 | 3036

BRAIN
A JOURNAL OF NEUROLOGY

A disease-specific metabolic brain network associated with corticobasal degeneration

Martin Niethammer,[1] Chris C. Tang,[1] Andrew Feigin,[1] Patricia J. Allen,[1] Lisette Heinen,[2] Sabine Hellwig,[3] Florian Amtage,[3] Era Hanspal,[4] Jean Paul Vonsattel,[5] Kathleen L. Poston,[6] Philipp T. Meyer,[7] Klaus L. Leenders[2] and David Eidelberg[1]

1 Centre for Neurosciences, The Feinstein Institute for Medical Research, Manhasset, NY 11030, USA
2 Department of Neurology, University Medical Centre Groningen, Groningen, The Netherlands
3 Department of Neurology, University Hospital Freiburg, Freiburg, Germany
4 Parkinson's Disease and Movement Disorders Centre, Albany Medical Centre, Albany, NY 12208, USA
5 The New York Brain Bank, Columbia Presbyterian Medical Centre, New York, NY 10032, USA
6 Department of Neurology and Neurological Sciences, Stanford University Medical Centre, Stanford, CA 94305, USA
7 Department of Nuclear Medicine, University Hospital Freiburg, Freiburg, Germany

Correspondence to: David Eidelberg, MD,
Centre for Neurosciences, The Feinstein Institute for Medical Research,
350 Community Drive, Manhasset, NY 11030, USA
E-mail: david1@nshs.edu

Corticobasal degeneration is an uncommon parkinsonian variant condition that is diagnosed mainly on clinical examination. To facilitate the differential diagnosis of this disorder, we used metabolic brain imaging to characterize a specific network that can be used to discriminate corticobasal degeneration from other atypical parkinsonian syndromes. Ten non-demented patients (eight females/two males; age 73.9 $\pm$ 5.7 years) underwent metabolic brain imaging with ^{18}F-fluorodeoxyglucose positron emission tomography for atypical parkinsonism. These individuals were diagnosed clinically with probable corticobasal degeneration. This diagnosis was confirmed in the three subjects who additionally underwent post-mortem examination. Ten age-matched healthy subjects (five females/five males; age 71.7 $\pm$ 6.7 years) served as controls for the imaging studies. Spatial covariance analysis was applied to scan data from the combined group to identify a significant corticobasal degeneration-related metabolic pattern that discriminated ($P < 0.001$) the patients from the healthy control group. This pattern was characterized by bilateral, asymmetric metabolic reductions involving frontal and parietal cortex, thalamus, and caudate nucleus. These pattern-related changes were greater in magnitude in the cerebral hemisphere opposite the more clinically affected body side. The presence of this corticobasal degeneration-related metabolic topography was confirmed in two independent testing sets of patient and control scans, with elevated pattern expression ($P < 0.001$) in both disease groups relative to corresponding normal values. We next determined whether prospectively computed expression values for this pattern accurately discriminated corticobasal degeneration from multiple system atrophy and progressive supranuclear palsy (the two most common atypical parkinsonian syndromes) on a single case basis. Based upon this measure, corticobasal degeneration was successfully distinguished from multiple system atrophy ($P < 0.001$) but not progressive supranuclear palsy, presumably because of the overlap (~24%) that existed between the corticobasal degeneration- and the progressive supranuclear palsy-related metabolic topographies. Nonetheless, excellent discrimination between these disease entities was achieved by computing hemispheric asymmetry scores for the corticobasal degeneration-related pattern on a prospective single scan basis. Indeed, a logistic algorithm based on the asymmetry scores combined with separately computed expression values for a previously validated progressive supranuclear palsy-related pattern provided excellent specificity (corticobasal degeneration: 92.7%; progressive supranuclear palsy: 94.1%) in classifying 58 testing subjects. In conclusion, corticobasal degeneration is associated with a reproducible disease-related metabolic covariance pattern that may help to distinguish this disorder from other atypical parkinsonian syndromes.

Received March 4, 2014. Revised July 14, 2014. Accepted July 25, 2014. Advance Access publication September 9, 2014

Keywords: brain networks; corticobasal degeneration; differential diagnosis; FDG PET; glucose metabolism

Abbreviations: CBD = corticobasal degeneration; CBDRP = corticobasal degeneration-related metabolic covariance pattern; FDG = ^{18}F-fluorodeoxyglucose; MSA = multiple system atrophy; PDCP = Parkinson's disease cognition-related metabolic covariance pattern; PDRP = Parkinson's disease motor-related metabolic covariance pattern; PSP = progressive supranuclear palsy; PSPRP = progressive supranuclear palsy-related metabolic covariance pattern

Introduction

Parkinsonism is characterized by a combination of clinical features that include tremor, bradykinesia, rigidity, and postural instability. Idiopathic Parkinson's disease is the most common cause of neurodegenerative parkinsonism, whereas atypical parkinsonian syndromes, also referred to as 'Parkinson plus syndromes,' encompass several specific diseases with distinct pathology and prognosis, including progressive supranuclear palsy (PSP), multiple system atrophy (MSA), and corticobasal degeneration (CBD). Atypical parkinsonian syndromes can represent as much as 15-20% of parkinsonism seen in specialty practice (Fahn *et al.*, 2004). Diagnosis of Parkinson's disease and atypical parkinsonism is made based on clinical examination, relying on established consensus criteria. Parkinson's disease and the different atypical parkinsonian syndromes can be differentiated by pathological examination, but post-mortem studies demonstrate only a 76% accuracy in the clinical diagnosis of Parkinson's disease (Hughes *et al.*, 2002). Although this accuracy does increase with longer follow-up evaluations by movement disorder specialists, it remains significantly lower for atypical syndromes (Hughes *et al.*, 2002).

Pathologically, CBD and PSP are classified as tauopathies with significant overlap in motor and cognitive deficits (Sha *et al.*, 2006), distinct from the alpha-synuclein aggregates that characterize Parkinson's disease and MSA (Poston, 2010). Clinically, CBD is characterized by asymmetric, levodopa non-responsive parkinsonism. The presentation typically includes progressive rigidity and limb apraxia, in conjunction with limb dystonia, stimulus-sensitive myoclonus, and/or cortical sensory loss (Boeve *et al.*, 2003). However, predominantly cognitive presentations are also seen (Litvan *et al.*, 1997; Mahapatra *et al.*, 2004; Hu *et al.*, 2009), potentially confounding the diagnosis.

With this in mind, one important aim of neuroimaging is to provide increased diagnostic accuracy, allowing for the selection of appropriate treatment strategies and more accurate long-term prognosis. Conventional neuroimaging such as MRI is of limited value in the diagnosis of the different atypical parkinsonian syndromes. Asymmetric atrophy of the premotor and parietal cortices is suggestive but neither sensitive nor specific for CBD, particularly at early disease stages (Mahapatra *et al.*, 2004). As Parkinson's disease and atypical parkinsonian syndromes are both associated with presynaptic nigrostriatal dopaminergic deficits, dopaminergic imaging has been of limited use in the differential diagnosis of these disorders (Vlaar *et al.*, 2007).

In contrast, functional imaging techniques aimed at measuring cerebral blood flow or metabolism have been used extensively to identify disease-specific changes in local neural activity (Eidelberg, 2009). In the past several years, voxel-based spatial covariance analysis has been successfully applied to ^{18}F-fluorodeoxyglucose (FDG) PET images to identify metabolic patterns relating to specific neurodegenerative diseases (Eidelberg, 2009). Using this approach, we have previously identified and validated patterns that can discriminate Parkinson's disease, MSA, and PSP not only from healthy subjects but also from each other (Spetsieris *et al.*, 2009; Tang *et al.*, 2010*b*; Niethammer and Eidelberg, 2012).

To date, we have not applied this network-based method to the study of CBD, although metabolic asymmetries can readily be seen in patients with this disorder (Eidelberg *et al.*, 1991). In the present study, we identified and validated a disease-specific metabolic pattern that can separate patients with CBD from healthy controls, and patients with other atypical parkinsonian syndromes.

Materials and methods

Subjects

Demographic data for the patient cohorts and the healthy control groups are presented in Table 1. Patients were referred to the respective institution to aid in clinical diagnosis between January 1995 and December 2006 (North Shore University Hospital, NY, USA), March 2009 and October 2010 (Stanford University, CA, USA), July 2008 and January 2011 (University of Freiburg, Freiburg, Germany), and between January 1998 and December 2008 (University Medical Centre Groningen, Groningen, The Netherlands). All patients had parkinsonian signs and were followed by movement disorder specialists at each institution for at least 6 months after PET imaging. Inclusion required a final clinical diagnosis of probable CBD, PSP, or MSA that was supported by the clinical impression of the trained movement disorder specialists, who evaluated the patients, chart review (M.N., K.L.P., E.H., L.H., K.L.L., S.H., F.A.) using published clinical criteria (Litvan, 2003; Poston, 2010; Armstrong *et al.*, 2013), and the absence of dementia as well as structural brain abnormalities on MRI (i.e. mass lesions, white matter changes, or ischaemia) that could have explained the clinical findings. Diagnosis was confirmed pathologically (J.P.V.) in 10 patients (three CBD, three PSP, and four MSA). Scan data from some of the patients have appeared previously as part of different analyses (Tang *et al.*, 2010*b*; Teune *et al.*, 2010; Hellwig *et al.*, 2012).

To identify a CBD-related metabolic covariance pattern (CBDRP), we studied 10 patients (CBD_{NS}: eight females/two males; age 73.9 ± 5.7 years (mean ± standard deviation [SD]); disease duration 3.5 ± 1.5 years; Table 2) who met diagnostic criteria for probable CBD, with limb asymmetry and apraxia on clinical examination and without evidence of eye movement abnormalities. Three of 10 subjects with CBD were pathologically confirmed cases. Eight of the patients with CBD in this group and 10 age-matched normal control subjects (NL_{NS}: five females/five males; age 71.7 ± 6.7 years) were scanned at North Shore University Hospital; two patients with CBD were scanned at Stanford University. Six of 10 patients with CBD had symptoms predominately on the right, and four on the left.

Table 1 Patient cohorts

Site	Category	*n*	Age (years)	Disease duration (years)
North Shore University Hospital/Stanford University (NS)	NL (NL_{NS})	10	71.7 ± 6.7	n/a
	CBD (CBD_{NS})	10	73.9 ± 5.7	3.5 ± 1.5
	PSP (PSP_{NS})	30	69.4 ± 5.6	2.7 ± 1.2
	MSA (MSA_{NS})	40	61.4 ± 8.7	3.9 ± 2.2
University Medical Centre Groningen (GR)	NL (NL_{GR})	10	65.0 ± 10.1	n/a
	CBD (CBD_{GR})	10	68.9 ± 9.3	2.0 ± 0.8
University of Freiburg (FR)	CBD (CBD_{FR})	7	65.8 ± 6.0	2.3 ± 1.6
	PSP (PSP_{FR})	21	70.5 ± 7.6	2.9 ± 2.0
	MSA (MSA_{FR})	12	65.1 ± 7.2	3.6 ± 2.0

Table 2 Patient characteristics: derivation cohort (CBD_{NS})

Subject No.	Gender	Age (years)	Disease duration (years)	Clinically worse side	Pathologically confirmed	CBDRP score (z-scored)
1	F	74.5	3	Left	Yes	5.02
2	F	61.9	1	Right	Yes	5.59
3	M	81.0	3	Right	Yes	12.01
4	F	78.2	2	Right	No	5.26
5	F	73.2	5	Right	No	6.41
6	F	77.6	6	Right	No	8.04
7	F	76.0	3	Right	No	4.07
8	F	72.5	6	Left	No	5.50
9	F	68.2	1	Left	No	8.14
10	M	79.2	5	Left	No	6.75

To validate the pattern, we studied independent testing cohorts of atypical parkinsonian syndromes subjects who had uncertain diagnoses at the time of FDG PET and were then followed clinically by movement disorder specialists for at least 6 months until a final clinical diagnosis was made. We studied 10 patients with CBD (CBD_{GR}: seven females/three males; age 68.9 ± 9.3 years; disease duration 2.0 ± 0.82 years) and 10 normal control subjects (NL_{GR}: five females/five males; age 65.0 ± 10.1 years) who were scanned with FDG PET at the University Medical Centre Groningen, The Netherlands. We also measured CBDRP expression in an additional testing cohort comprised of seven patients with CBD (CBD_{FR}: age 65.8 ± 6.0 years; disease duration 2.3 ± 1.6 years) who were scanned with FDG PET at the University of Freiburg, Germany. CBD patients in both cohorts were scanned with an unverified diagnosis of atypical parkinsonian syndromes, and only confirmed as CBD on clinical follow-up (3.0 ± 1.0 years for CBD_{GR} and 1.0 ± 0.6 years for CBD_{FR}) (Teune *et al.*, 2010; Hellwig *et al.*, 2012).

To examine pattern expression in other atypical parkinsonian disorders, we studied a cohort comprised of patients clinically diagnosed with PSP (PSP_{NS}: $n = 30$; age 69.4 ± 5.6 years; disease duration 2.7 ± 1.2 years) or MSA (MSA_{NS}: $n = 40$; age 61.4 ± 8.7 years; disease duration 3.9 ± 2.2 years) who were scanned with FDG PET at North Shore University Hospital. Among these patients, three cases with PSP and four MSA cases were pathologically confirmed. We also studied an additional atypical parkinsonian syndromes cohort comprised of patients diagnosed with PSP (PSP_{FR}: $n = 21$; age 70.5 ± 7.6 years; disease duration 2.9 ± 2.0 years) or MSA (MSA_{FR}: $n = 12$; age 65.1 ± 7.2 years; disease duration 3.6 ± 2.0 years) who were scanned at the University of Freiburg. All of these patients had uncertain diagnoses of atypical parkinsonian syndromes at the time of imaging, and their final clinical diagnoses were made after clinical follow-up (PSP_{NS}: 1.9 ± 1.1 years; PSP_{FR}: 1.0 ± 0.4 years; MSA_{NS}: 3.2 ± 2.6 years; MSA_{FR}: 0.8 ± 0.3 years) (Tang *et al.*, 2010*b*; Hellwig *et al.*, 2012).

Ethical permission for the procedures was obtained from the Institutional Review Board at North Shore University Hospital and Stanford University, and the local ethics committee at University of Freiburg and the University Medical Centre Groningen. Written consent was obtained at each institution from each subject following detailed explanation of the scanning procedures.

PET

All subjects were scanned with FDG PET under resting conditions. All anti-parkinsonian medications were withheld at least 12 h before imaging. PET imaging was performed using a GE Advance tomograph [4.0 mm, full-width at half-maximum (FWHM), North Shore University Hospital], a GE PET/CT Discovery LS (5 mm FWHM, Stanford University), a Siemens ECAT HR+ PET scanner (4.1 mm FWHM, University Medical Centre Groningen), or a Siemens ECAT EXACT 922/47 scanner (5.5 mm FWHM; University of Freiburg) as described previously (Huang *et al.*, 2007; Teune *et al.*, 2010; Meyer *et al.*, 2011). Scans from each subject were realigned and spatially normalized to a standard Talairach-based FDG PET template, and smoothed with an isotropic Gaussian kernel (10 mm) in all directions to improve the signal-to-noise ratio (Feigin *et al.*, 2007; Huang *et al.*, 2007). All image processing was performed using Statistical Parametric Mapping (SPM5) software (Wellcome Department of Cognitive Neurology, London, UK) running in MATLAB (MathWorks).

Network analysis

CBDRP identification

To identify a specific metabolic pattern associated with CBD, we applied a spatial covariance mapping algorithm (Eidelberg, 2009; Niethammer and Eidelberg, 2012; Spetsieris *et al.*, 2013) to the FDG PET data from the 10 CBD_{NS} patients and 10 NL_{NS} subjects that comprised the derivation set. This method is based on a principal component analysis that can be used to identify specific disease-related spatial covariance patterns with significantly greater expression (denoted by higher subject scores) in patients than in control subjects. A detailed description of this approach has appeared elsewhere (Habeck and Stern, 2010; Spetsieris and Eidelberg, 2011). In brief, principal component analysis was performed on scans from the

combined group of patients and normal controls ($n = 20$) using an automated voxel-based routine (software freely available at http://feinsteinneuroscience.org/imaging-software) in a common stereotaxic space. The combination of principal component patterns that best discriminated patients from controls in the derivation set was identified using pre-specified subject score criteria (Spetsieris and Eidelberg, 2011). To delineate a specific CBD-related topography, we limited the analysis to the set of principal components that in aggregate accounted for the top 50% of subject × voxel variability, and for which each individual principal component contributed at least 10% to the total variance in the scan data. Region weights for the resulting disease-related topography (denoted by voxel loadings on the pattern) were tested for reliability using bootstrap resampling (Habeck and Stern, 2010). Coordinates were reported in the standard anatomical space developed at the Montreal Neurological Institute. The cytoarchitectonic localization of each reported network-related region was confirmed using the Talairach space utility available at http://www.ihb.spb.ru/~pet_lab/TSU/TSUMain.html. For pattern derivation, the scans from the CBD patients with predominantly left-sided symptoms were flipped so that all subjects had the left hemispheres of the brain as their most affected side.

CBDRP validation

Following derivation, the CBDRP candidate network was validated by computing its expression in patient and control testing data from the CBD_{GR}, CBD_{FR}, and NL_{GR} cohorts. The Freiburg data set did not include scans from healthy control subjects. As in the derivation set, scans of patients with CBD with predominantly left-sided symptoms in the testing cohorts were flipped so that the most affected hemisphere was on the left side. Subject scores for the candidate CBDRP identified in the derivation set were computed in the testing scans using an automated voxel-based algorithm to quantify the expression of known patterns on a prospective single scan basis (Spetsieris *et al.*, 2006, 2013; Eidelberg, 2009) and were compared across groups. In addition, CBDRP expression values were computed in scans from the testing cohorts with PSP (PSP_{NS} and PSP_{FR}) or MSA (MSA_{NS} and MSA_{FR}). The resulting subject scores were compared with values from the corresponding CBD cohorts (CBD_{NS} and CBD_{FR}).

CBDRP asymmetry index

To obtain a quantitative measure of the pattern asymmetry in individual subjects, we generated a hemi-CBDRP from the left side (most affected hemisphere) of the whole-brain pattern. For each subject, hemi-CBDRP expression values were computed separately for the two hemispheres (hemi-CBDRP was flipped to calculate the value for the right hemisphere). The difference in hemispheric values was calculated and used as an asymmetry index of CBDRP expression. Values from the diagnostically relevant patient groups (CBD and PSP) were compared with each other and with measures from the healthy volunteer group.

Differential diagnosis

In addition to assessing group differences in the expression of covariance patterns relating to CBD and PSP in the testing populations, we developed an automated logistic algorithm to discriminate between these disorders at the individual patient level. To this end, we extended the pattern-based classification strategy that we previously developed to distinguish patients with Parkinson's disease from MSA and PSP (Tang *et al.*, 2010*b*). A training sample was constructed using scans from the 10 CBD_{NS} subjects used for CBDRP derivation (age 73.9 ± 5.7 years) and scans from 10 PSP_{NS} patients (age 69.9 ± 8.2 years) closely matched in age to their CBD_{NS} counterpart subjects. Logistic regression analysis was performed on the scan data from this combined training sample to determine which of the three network measures [i.e. CBDRP expression, CBDRP asymmetry index, and PSP-related metabolic covariance pattern (PSPRP) expression] could, singly or in combination, best differentiate between the two diseases. The model with the best between-group discrimination was selected based on the lowest Akaike information criterion value (Burnham and Anderson, 2002).

For validation, this algorithm was used prospectively to classify each of 58 independent subjects. This testing set was comprised of 17 CBD (10 CBD_{GR} and seven CBD_{FR}) and 41 PSP patients (20 remaining PSP_{NS} and 21 PSP_{FR}). For each subject, probability values for CBD (P_{CBD}) or PSP (P_{PSP}) were computed using the original logistic equation from the training sample and then compared to the optimal cut-off probabilities for classifying a given subject as CBD or PSP (i.e. cut-off_{CBD} or cut-off_{PSP}). The cut-off probability for each condition was determined by identifying an inflection point on each receiver-operating characteristic (ROC) curve corresponding to high specificity and sensitivity (Tang *et al.*, 2010*b*). Because in a clinical setting FDG PET is used primarily as a confirmatory test rather than for screening, high specificity (i.e. >90%) rather than high sensitivity was preferred in determining a suitable inflection point for each curve and, correspondingly, the cut-off probability for each disease. By comparing the individual case probabilities (P_{CBD} and P_{PSP}) to the cut-off probabilities, each subject was classified as CBD if $P_{CBD} >$ cut-off_{CBD}, *P*SP if $P_{PSP} >$ cut-off_{PSP}, or as an indeterminate case if $P_{CBD} \leqslant$ cut-off_{CBD} and $P_{PSP} \leqslant$ cut-off_{PSP}. We then calculated discriminative measures (sensitivity, specificity, positive predictive value and negative predictive value) for the CBD and PSP groups.

Statistical analysis

Because of the relatively small sample size of some groups (e.g. $n = 7$ in CBD_{FR}), the non-normal distribution of the data in some groups, and unequal sample sizes, non-parametric tests were used to compare network measures between (Mann-Whitney U-tests) and among (Kruskal-Wallis tests) the different groups. For all patients and control subjects, individual pattern scores were standardized (*z*-scored) with respect to the original NL_{NS} group used in pattern derivation. Thus, for each of these normal reference samples, mean pattern expression was zero with an SD of one. Logistic regression analysis was performed in SAS 9.2 (SAS Institute Inc.) and other statistical tests were performed in SPSS 14.0 (SPSS Inc.). All tests were considered significant for $P < 0.05$.

Results

Corticobasal degeneration-related metabolic pattern

Spatial covariance analysis of the metabolic imaging data from the derivation set revealed a significant CBDRP (principal component 1, accounting for 18.4% of the total subject × voxel variance of the data). This pattern (Fig. 1A and Table 3) was characterized by metabolic reductions in the primary motor (BA4), lateral premotor (BA6), prefrontal (BA9) and parietal (BA40) cortical regions, cingulate gyrus (BA24, BA31) and in the thalamus (mediodorsal, ventrolateral and lateroposterior nuclei). The changes in these

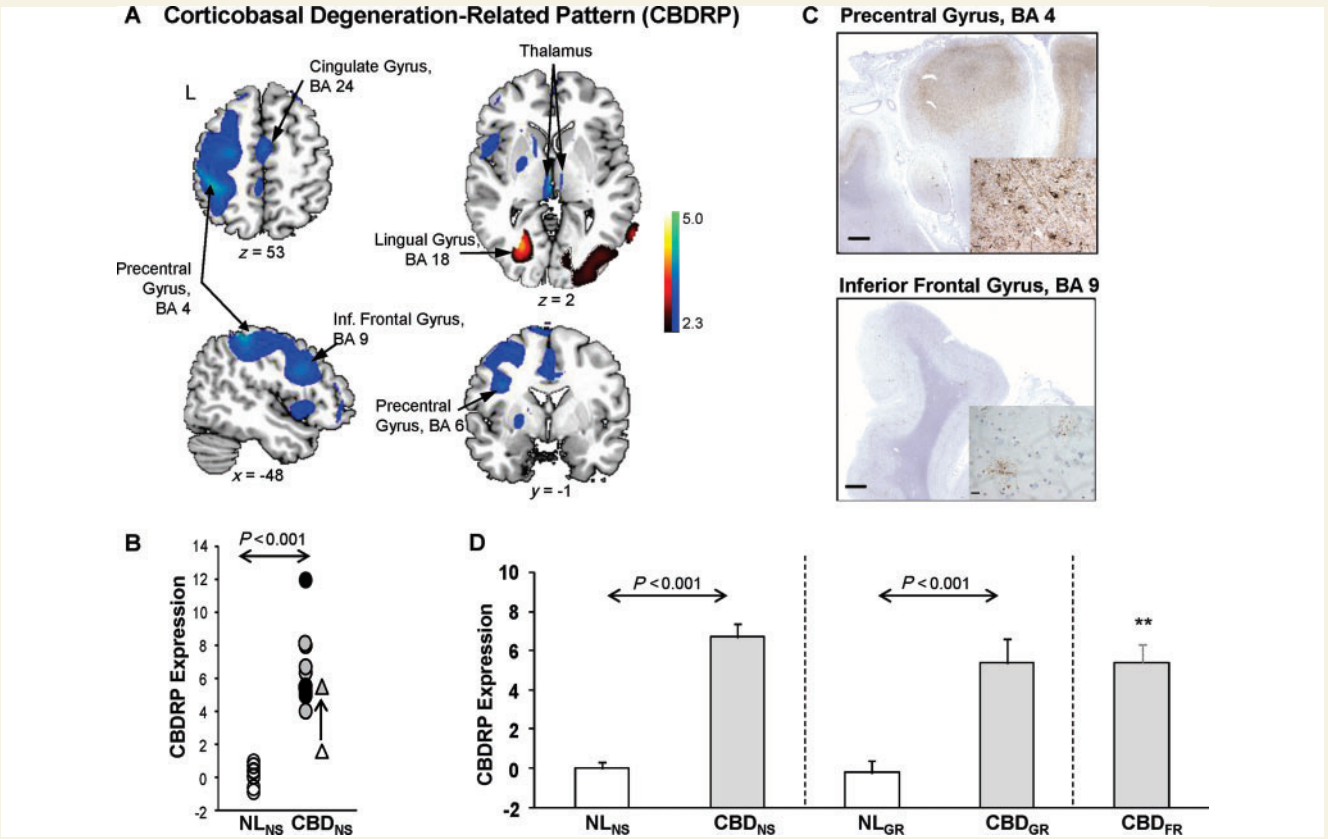

Figure 1 Corticobasal degeneration-related pattern. (**A**) Corticobasal degeneration-related pattern (CBDRP) identified by spatial covariance analysis of FDG PET scans from a derivation cohort of 10 patients with CBD and 10 normal control (NL) subjects scanned at the North Shore University Hospital (eight CBD and 10 control subjects) and Stanford University (two CBD subjects). This pattern was characterized by metabolic reductions in the left frontal and parietal lobes, precentral gyrus, thalamus, and caudate head, associated with increased metabolism in the left occipital lobe, left lingual gyrus, right occipital lobe and right inferior occipital gyrus. [The display represents regions that contributed significantly to the network at $Z = 2.33$ ($P < 0.01$) and were demonstrated to be reliable ($P = 0.01$; 1000 iterations) by bootstrap resampling. Voxels with positive region weights (metabolic increases) are colour-coded red and those with negative region weights (metabolic decreases) are colour-coded blue. Left hemisphere is labelled as 'L']. (**B**) In this derivation sample, individual CBDRP expression significantly ($P < 0.001$, permutation test) separated the 10 patients with CBD (CBD_{NS}; filled circles) from the 10 normal controls (NL_{NS}; open circles). The three pathologically confirmed cases are indicated by black filled circles. One subject with CBD also had undergone FDG PET 3 years before the scan included in the derivation sample. For this subject, CBDRP expression was 1.64 at the initial scan, and was then increased to 5.50 3 years later when the same subject carried a diagnosis of CBD (open and filled triangles, respectively). (**C**) *Top:* Cortico-subcortical micrograph of the precentral gyrus (BA4) from a section stained with AT8 antibodies directed against phosphorylated tau. On general survey, the labelling was diffuse, blurring the cortico-subcortical demarcation. *Inset*: Strong labelling was seen of neuropil threads, astrocytes, and scattered neurons. *Bottom*: Cortico-subcortical micrograph from the same specimen showing AT8 staining in the inferior frontal gyrus (BA9). *Inset*: In contrast to BA4, the cortico-subcortical demarcation is discrete and the tauopathic burden consists only of occasional astrocytic plaques and rare neuropil threads. Scale bars = 1.0 cm; inset = 15 μm. (**D**) Validation of CBDRP in two independent testing cohorts: CBD_{GR} (10 patients with CBD and 10 age-matched normal controls scanned at University Medical Centre Groningen) and CBD_{FR} (seven patients with CBD scanned at the University of Freiburg). As in the derivation CBD_{NS} cohort (*left*; $P < 0.001$, Mann-Whitney test), pattern expression was significantly elevated in the CBD_{GR} patients compared to the NL_{GR} controls (*middle*; $P < 0.001$). Likewise, pattern expression in CBD_{FR} (*right*) was significantly elevated relative to both the NL_{NS} ($P = 0.001$) and NL_{GR} ($P < 0.001$) groups. Indeed, average elevation of CBDRP expression was not different ($P = 0.55$, Kruskal-Wallis test) between the derivation and the two validation CBD groups. Error bars represent SE. $^{**}P \leqslant 0.001$, Mann-Whitney tests, compared to normal control subjects (NL).

network regions were more pronounced in the left hemisphere (i.e. opposite the more affected body side), although abnormal changes were also present in the other hemisphere, albeit at lower significant levels (not shown in Fig. 1A). Voxel weights on CBDRP were stable in these regions (inverse coefficient of variation range = −2.22 to 2.26, $P = 0.01$; bootstrap estimation, 1000 iterations). In the derivation set, pattern expression values (Fig. 1B and D) significantly separated the patients with CBD from the healthy control subjects ($P < 0.001$; permutation test). The clinical diagnosis of CBD was confirmed post-mortem in three of 10 subjects (Fig. 1B and Table 2) used to identify the pattern. In each of the autopsied cases, subject scores were

Table 3 Brain regions with significant contributions to the CBD-related pattern

Brain region	Coordinates[a]			Z_{max}
	x	y	z	
Network-related metabolic reductions (negative region weights)				
Thalamus MD/VL/LP nuclei,				
Left	−2	−22	2	3.50
Right	6	−14	−2	2.53
Left inferior parietal lobule, BA40	−44	−38	56	3.22
Left precentral gyrus, BA4/6	−32	−16	68	3.19
	−40	2	28	2.88
Left cingulate gyrus, BA31	−10	−24	40	2.89
Left inferior frontal gyrus, BA9	−52	14	28	2.80
Left middle frontal gyrus, BA6	−28	16	62	2.67
Left cingulate gyrus, BA24	−8	−8	40	2.66
Network-related metabolic increases (positive region weights)				
Left lingual gyrus, BA18	−26	−70	4	3.20
Right inferior occipital gyrus, BA18	40	−92	−18	2.83
Right lingual gyrus, BA17	20	−102	−16	2.77

[a] Montreal Neurological Institute standard space.
MD = mediodorsal; VL = ventrolateral; LP = lateroposterior; BA = Brodmann area.

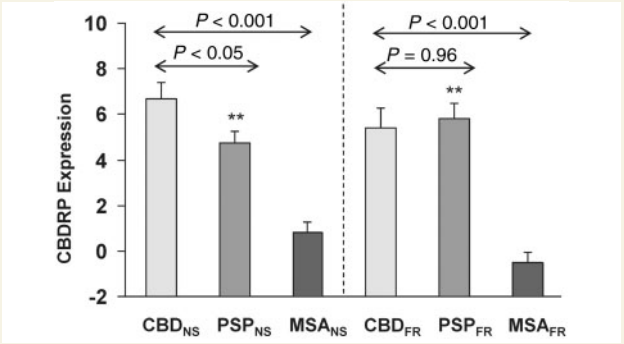

Figure 2 CBDRP expression in atypical parkinsonian syndromes. *Left:* CBDRP expression in 10 patients with CBD (CBD_{NS}), 30 patients with PSP (PSP_{NS}) and 40 patients with MSA (MSA_{NS}) scanned with FDG PET at the North Shore University Hospital. The patients in the CBD_{NS} group showed higher CBDRP expression than both the PSP_{NS} ($P < 0.05$; Mann-Whitney test) and MSA_{NS} ($P < 0.001$) patient groups. *Right:* CBDRP expression in independent groups of seven CBD (CBD_{FR}), 21 PSP (PSP_{FR}) and 12 MSA (MSA_{FR}) patients scanned with FDG PET at the University of Freiburg. In these groups, CBDRP expression was significantly elevated in the patients with CBD compared with the patients with MSA ($P < 0.001$; Mann-Whitney test), but was not different from the patients with PSP ($P = 0.96$). In addition, both PSP_{NS} and PSP_{FR} patients showed higher CBDRP expression ($P < 0.001$; Mann-Whitney test) than the normal (NL_{NS}) control subjects. Error bars represent SE. $^{**}P \leqslant 0.001$, Mann-Whitney tests, compared to normal control subjects.

>5.0 SD (range 5.0–12.0) above the normal mean value. The pathological representation of an autopsied case who had the highest CBDRP score (12.01) is shown in Fig. 1C. Of note, one of the CBD patients (Fig. 1B) had undergone FDG PET 3 years before the scan used in pattern identification. At that time, the clinical diagnosis was one of focal dystonia, without accompanying parkinsonism or cortical sensory findings. In this subject, CBDRP expression was 1.64 at the initial scan, but increased to 5.5 (Fig. 1B) after 3 years, by which time a clinical diagnosis of CBD had been made.

Pattern validation

To validate the CBDRP, we prospectively computed the expression of this pattern in an independent testing cohort comprised of 10 patients with CBD (CBD_{GR}) and 10 age-matched normal control subjects (NL_{GR}) scanned at University Medical Centre Groningen. Subject scores for this pattern were computed on a prospective single scan basis in each of testing scans using an automated voxel-based algorithm that was blind to diagnostic category (i.e. CBD_{GR} or NL_{GR}). In this testing sample (Fig. 1D) CBDRP expression was also elevated ($P < 0.001$; Mann-Whitney test) in the patients (CBD_{GR}) relative to the healthy (NL_{GR}) control subjects. Of note, subject scores in both cohorts were standardized with respect to CBDRP expression values from the healthy NL_{NS} subjects in the derivation sample. Nevertheless, the mean for the prospectively computed NL_{GR} values (−0.24) was near the zero mean ($P = 0.36$, Mann-Whitney test) that was set for the NL_{NS} (see 'Materials and methods' section).

Lastly, we computed CBDRP expression in an additional testing cohort comprised of seven patients with CBD (CBD_{FR}) scanned at the University of Freiburg. Although no scans from healthy control subjects were available at this site, subject scores for CBD_{FR} patients (Fig. 1D) were significantly elevated ($P \leqslant 0.001$, Mann-Whitney test) relative to healthy NL_{NS} and NL_{GR} control values. Indeed, the expression of this pattern in CBD_{FR} patients (CBD_{FR}: 5.39 ± 0.89) did not differ ($P = 0.55$; Kruskal-Wallis test) from corresponding measurements in CBD_{NS} and CBD_{GR} patients [CBD_{NS}: 6.68 ± 0.72 (derivation); CBD_{GR}: 5.35 ± 1.27].

CBDRP expression in other forms of atypical parkinsonism

To determine the specificity of the pattern for CBD, we measured its expression in other forms of atypical parkinsonian syndromes. Specifically, we quantified CBDRP scores in 30 PSP patients (PSP_{NS}) and 40 MSA patients (MSA_{NS}) scanned at North Shore University Hospital. The patients in the CBD_{NS} group (Fig. 2) had greater CBDRP expression than either the PSP_{NS} ($P < 0.05$) or the MSA_{NS} ($P < 0.001$; Mann-Whitney tests) groups. We also computed CBDRP expression values in 21 patients with PSP and 12 with MSA scanned at the University of Freiburg, designated as PSP_{FR} and MSA_{FR}, respectively. CBDRP expression (Fig. 2) was also elevated in CBD_{FR} compared with MSA_{FR}. However, CBDRP scores in the CBD_{FR} patients did not differ ($P = 0.96$) from those computed in their PSP_{FR} counterparts. Moreover, PSP_{NS} and PSP_{FR} subjects had greater CBDRP expression ($P < 0.001$; Mann-Whitney tests) than NL_{NS} or NL_{GR} control values. Thus, while confirming the presence of abnormal increases in CBDRP expression in

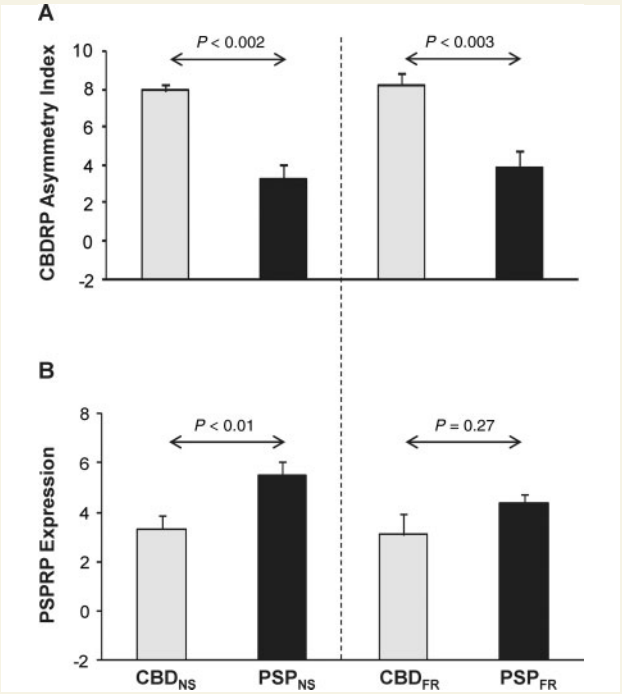

Figure 3 CBDRP asymmetry index and PSPRP expression. (**A**) The CBDRP asymmetry index was found to be greater in both CBD patient cohorts (CBD_{NS} versus PSP_{NS}: $P < 0.002$; CBD_{FR} versus PSP_{FR}: $P < 0.003$; Mann-Whitney tests) than for the respective PSP patient cohorts. (**B**) Expression of a previously identified PSP-related pattern (PSPRP) (Eckert *et al.*, 2008) was significantly higher in the PSP_{NS} group relative to the CBD_{NS} group ($P < 0.01$; Mann-Whitney test), but was not different between the PSP_{FR} and CBD_{FR} groups ($P = 0.27$). Error bars represent SE.

multiple prospective CBD cohorts, the testing data also revealed significant pattern elevations in PSP patients.

CBDRP asymmetry index and PSPRP expression

We used the inherent asymmetries that characterize the CBDRP topography to define a hemispheric pattern. The hemi-CBDRP topography was defined by the left hemisphere of the original whole-brain pattern. As the side opposite the more affected limbs in patients with CBD, the left hemisphere contained the bulk of the local metabolic reductions that constitute this disease topography. The expression of the left hemi-CBDRP was separately computed in the two hemispheres of each subject (see 'Materials and methods' section). The left-right difference in these values was used to compute a CBDRP asymmetry index for each subject. Relative to the normal control group (NL_{NS}), the asymmetry index was greater in the CBD (CBD_{NS}: $P < 0.001$; CBD_{FR}: $P < 0.001$; Mann-Whitney tests) and the PSP (PSP_{NS}: $P < 0.005$; PSP_{FR}: $P = 0.005$; Mann-Whitney tests) samples. However, unlike the original whole-brain pattern, the CBDRP asymmetry index (Fig. 3A) was significantly greater in CBD relative to PSP in both differential diagnosis sets ($P \leqslant 0.003$ for CBD_{NS} versus PSP_{NS} and CBD_{FR} versus PSP_{FR}).

We also computed PSPRP expression in each of these subjects. PSPRP scores were indeed elevated in both PSP groups ($P < 0.001$; Mann-Whitney tests for PSP_{NS} versus NL_{NS} and PSP_{FR} versus NL_{NS}), and also in the two CBD samples ($P < 0.005$ for CBD_{NS} versus NL_{NS}; $P = 0.07$ for CBD_{FR} versus NL_{NS}). Moreover, PSPRP expression was significantly higher in PSP_{NS} compared to CBD_{NS} (Fig. 3B, *left*; $P < 0.01$), but was not different for the PSP_{FR} and CBD_{FR} groups (Fig. 3B, *right*; $P = 0.27$). Indeed, voxel-wise correlation of CBDRP and PSPRP revealed moderate overlap between the two patterns ($R^2 = 0.24$, $P < 0.001$). There was also a significant correlation between expression of CBDRP and PSPRP in individual subjects with CBD (Spearman's $r = 0.58$, $P = 0.001$, $n = 27$; combined group of CBD_{NS}, CBD_{GR} and CBD_{FR}) or PSP (Spearman's $r = 0.57$, $P < 0.001$, $n = 51$; combined group of PSP_{NS} and PSP_{FR}). These findings suggest that, singly, the two whole-brain network measures are insufficient for prospective discrimination between the two diseases. That said, adequate differentiation between these conditions may be possible using multiple network measures in combination.

Automated algorithm for differential diagnosis of corticobasal degeneration versus progressive supranuclear palsy

For accurate differential diagnosis of CBD and PSP, we next employed a logistic classification algorithm to determine whether the three network measures (the whole-brain CBDRP expression, the CBDRP asymmetry index, and the whole-brain PSPRP expression), individually or in combination, provided accurate discrimination between clinically diagnosed CBD and PSP patients at the single case level. In the training sample comprised of the 10 CBD_{NS} and the 10 age-matched PSP_{NS} cases (Fig. 4A), a logistic regression model based on the CBDRP asymmetry index and whole-brain PSPRP expression values produced better group separation ($\chi^2 = 15.6$, $P = 0.0004$; likelihood ratio test) than any individual univariate model as well as the other multivariate models. Receiver-operating characteristic (ROC) analysis of this selected bivariate model revealed that the area under-the-curve (AUC) was 0.94 ($P < 0.0001$), indicating excellent differentiation between the CBD and PSP patients. Odds ratio estimates for this model were 1.84 [95% confidence interval (CI) = 1.06–3.20, $P = 0.03$] for CBDRP asymmetry and 0.42 (95% CI = 0.15–1.19, $P = 0.10$) for PSPRP expression. Thus, greater asymmetry occurring in concert with lower PSPRP expression suggests a higher likelihood of CBD relative to PSP in a given subject.

To validate this algorithm, we applied the discriminant function of the model prospectively to individual subjects in an independent testing set of 17 CBD ($CBD_{GR} + CBD_{FR}$) and 41 PSP ($PSP_{NS} + PSP_{FR}$) subjects (Fig. 4B). The classification probabilities of CBD and PSP in each case were computed using the algorithm with the individual CBDRP asymmetry index and the whole-brain PSPRP expression value for that individual. The probabilities of all subjects were illustrated in a frequency distribution diagram

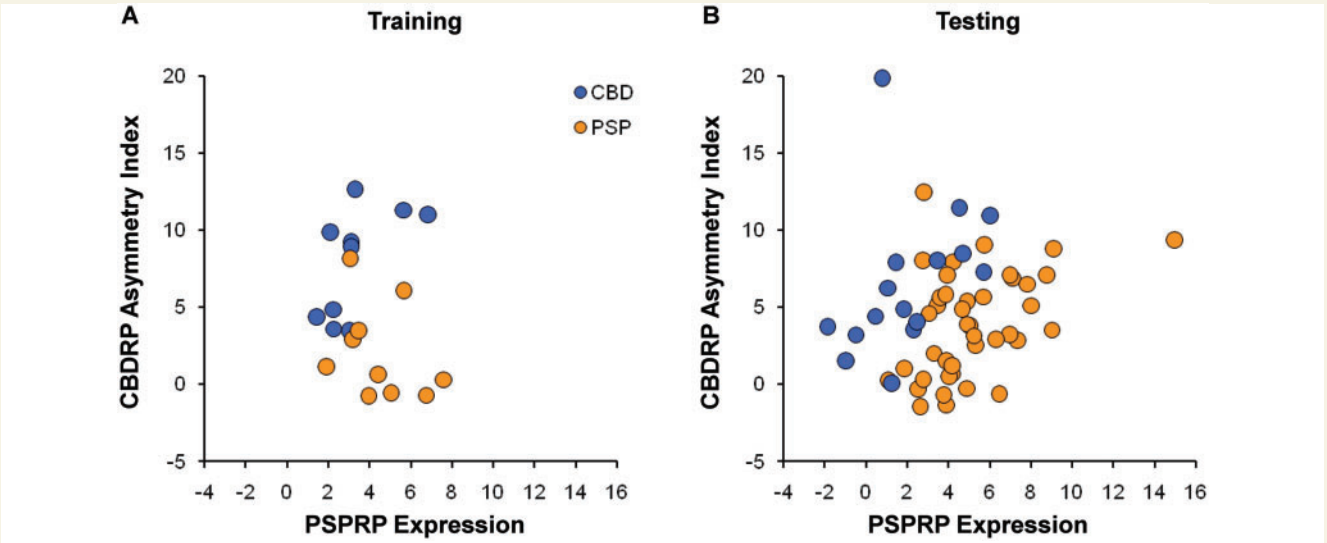

Figure 4 CBDRP asymmetry index and PSPRP expression in individual CBD and PSP patients. (**A**) Using logistic regression analysis, we found that a discriminant function using CBDRP asymmetry index and PSPRP expression resulted in the best differentiation between CBD_{NS} and PSP_{NS} ($\chi^2 = 15.6$, $P = 0.0004$; likelihood ratio test) (see text). Scatter plot displays the CBDRP asymmetry index and PSPRP expression in the training sample of 10 patients with CBD and 10 age-matched patients with PSP. (**B**) The automated algorithm for differential diagnosis was prospectively validated on a case-by-case basis in a testing sample of 58 patients, including 17 patients with CBD and 41 patients with PSP (see text). Scatter plot displays the CBDRP asymmetry index and PSPRP expression for these patients. In both plots, CBD and PSP patients are indicated by blue and orange circles, respectively.

(Fig. 5A). The subjects with higher CBD probabilities clustered on the right and those with higher PSP probabilities clustered on the left. ROC curve analysis (Fig. 5B) further revealed an AUC of 0.92 ($P < 0.0001$) indicating a high accuracy for the correct classification of CBD and PSP subjects. Based on these curves, the optimum cut-off probability for classifying CBD was 0.78 and for PSP was 0.63. Thus, patients whose probability values for CBD were >0.78 were classified as CBD and those whose probability values for PSP were >0.63 as PSP; patients whose probability values for CBD and PSP were both lower than their corresponding cut-off values were classified as indeterminate.

The image-based classification for each testing subject was compared to the ultimate clinical diagnosis of that individual. For the subjects diagnosed clinically with CBD, the image-based classifications had sensitivity of 76.5% (13/17, number of subjects), specificity of 92.7% (38/41), positive predictive value of 81.3% (13/16), and negative predictive value of 90.5% (38/42). For the PSP patients, the imaging classifications had 78.0% (32/41) sensitivity, 94.1% (16/17) specificity, 97.0% (32/33) positive predictive value, and 64.0% (16/25) negative predictive value. Nine of 58 testing subjects (15.5%) were classified as indeterminate by comparison of their probability values with the corresponding cut-offs. Of these, six were ultimately diagnosed as having PSP and three as CBD.

Discussion

In this study, we describe and validate a specific metabolic covariance pattern associated with CBD, termed CBDRP. Expression of this pattern reliably differentiated patients with clinical CBD from healthy control subjects in two independent samples. The CBDRP metabolic topography characterized by asymmetrical reductions (worse in the left hemisphere, i.e. contralateral to the more affected body side) in the cerebrum, lateral parietal and frontal regions and thalamus, with relative bilateral increases in occipital regions. This abnormal spatial covariance topography is consistent with previously reported metabolic (Eidelberg *et al.*, 1991; Eckert *et al.*, 2005; Teune *et al.*, 2010; Hellwig *et al.*, 2012; Zhao *et al.*, 2012) and structural (Soliveri *et al.*, 1999; Boxer *et al.*, 2006; Erbetta *et al.*, 2009) imaging changes in CBD identified using simple region-level analytical methods. Indeed, the pattern reflects the often marked asymmetry that is characteristic of the clinical presentation of CBD (Poston, 2010).

We acknowledge that derivation of a disease-specific pattern has to rely on the accuracy of the clinical diagnosis. This may be particularly problematic in CBD, where patients with the clinical diagnosis of CBD may be found to have another underlying pathology on post-mortem examination, mainly PSP, but including Alzheimer's disease, vascular parkinsonism, and Pick's disease (Litvan *et al.*, 1997; Josephs *et al.*, 2006; Hu *et al.*, 2009). This has prompted some investigators to propose the term corticobasal syndrome to describe the clinical findings in living patients, while reserving CBD for the definitive diagnosis made at post-mortem. That said, to derive and validate a metabolic pattern that is highly specific to CBD, we only included probable CBD patients who had parkinsonism with limb asymmetry and apraxia on clinical examination, without extraocular movement abnormalities (Litvan *et al.*, 1997). Thus, it is likely that the majority of the patients in our cohorts did indeed have CBD, as was confirmed by post-mortem examination of the brains of three of the patients whose scans were used to derive the CBDRP metabolic topography.

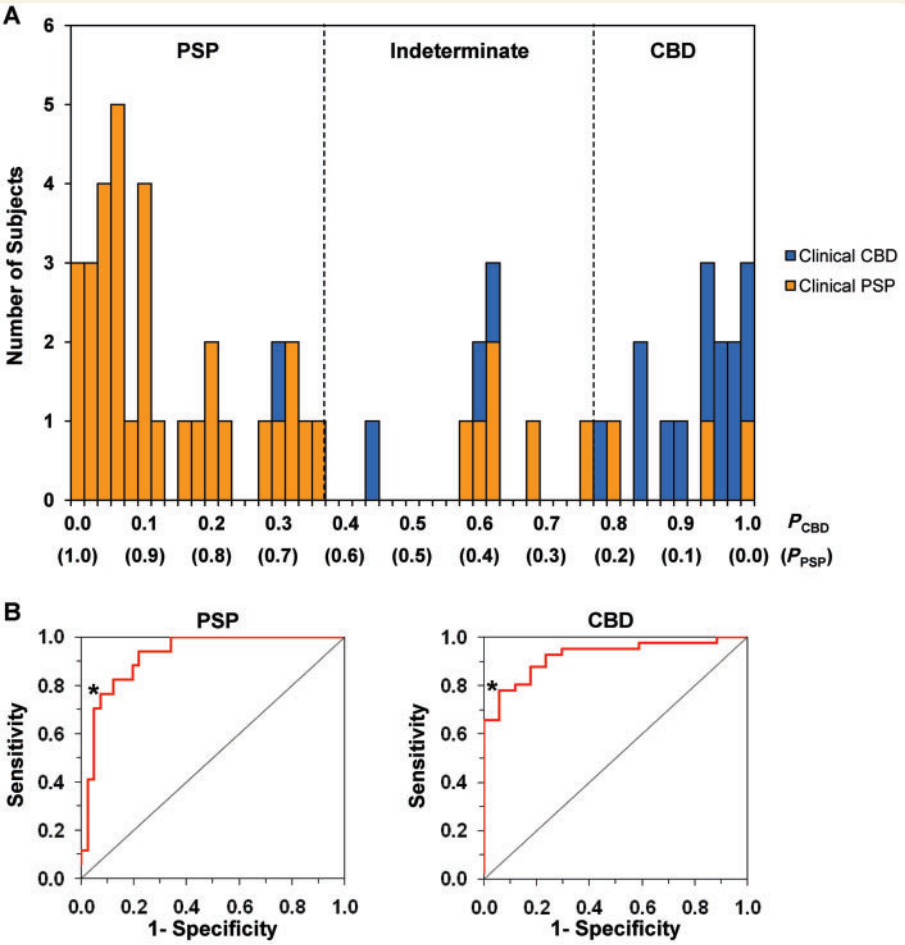

Figure 5 Results of the automated algorithm for differential diagnosis between CBD and PSP. (**A**) Frequency distribution diagram illustrating the disease probabilities of CBD and PSP calculated for the 58 subjects (17 CBD and 41 PSP) in the testing sample. Individual patients were classified as having CBD if the probability value for CBD (P_{CBD}) was >0.78 (i.e. cut-off$_{CBD}$; 16 subjects located to the right of the right dotted line), and as PSP if the probability value for PSP (P_{PSP}) was >0.63 (i.e. cut-off$_{PSP}$; 33 subjects located to left of the left dotted line). Patients whose probability values for CBD and PSP were both lower than their corresponding cut-off probabilities were classified as indeterminate cases, i.e. nine subjects located between the left and right dotted lines. The final clinical diagnoses of CBD and PSP patients are indicated by blue and orange bars, respectively. (**B**) Based on the receiver-operating characteristic (ROC) analysis for all patients in the testing sample, the area-under-the-curve (AUC) for PSP (*left*) and CBD (*right*) was 0.92 ($P < 0.0001$), consistent with that (0.94, $P < 0.0001$; not shown) of the training sample. The cut-off probability of each disease was determined based on the inflection point (asterisk) on each curve corresponding to the high specificity and sensitivity for classifying individual patients with each disease.

The clinical presentation of CBD may be quite heterogeneous. Indeed, the specific CBDRP topography described in this study may not be a consistent feature of variant phenotypes of the disorder, such as those with early dementia, which can be confused with Alzheimer's disease (Alexander *et al.*, 2014). Validation of this pattern as a specific diagnostic tool for CBD will ultimately be dependent on the accrual of additional cases with pathological confirmation. A separate possible problem is the low sensitivity in the diagnosis, a situation where neuroimaging could potentially be of benefit. It is well recognized that patients with the pathological diagnosis of CBD frequently may have different clinical syndromes and the true diagnosis is missed, as can occur in individuals diagnosed clinically as having PSP, Alzheimer's disease, progressive aphasia, symmetrical parkinsonism, or frontotemporal dementia (Litvan *et al.*, 1997; Hu *et al.*, 2009; Boeve, 2011; Hassan *et al.*, 2011). To assess the use of CBDRP expression in this context, it will be necessary to identify patients with pathologically confirmed CBD but with a different clinical diagnosis – and who had also undergone metabolic imaging in life.

In our cohorts, CBDRP expression was abnormally elevated in established CBD patients compared with healthy control subjects. Interestingly, one patient did undergo imaging twice. At the first time point, the clinical diagnosis was one of focal dystonia, without other features of CBD. CBDRP expression at the time was mildly elevated, only to become significantly elevated 3 years later, when the clinical diagnosis was established. We have previously shown that in Parkinson's disease, expression of motor- and cognition-related patterns (PDRP and PDCP, respectively) increase in individual patients over time (Huang *et al.*, 2007; Tang *et al.*, 2010*a*). Indeed, expression of PDCP is within the normal range

early in the disease course (Tang *et al.*, 2010*a*). Our finding in this one patient, coupled with a similar report in two patients with MSA (Poston *et al.*, 2012), suggests that disease-specific patterns may be useful markers of disease progression in individual patients in all forms of neurodegenerative parkinsonism. Nevertheless, longitudinal studies will be required to confirm this finding. Given the clinical uncertainty early in the disease process, it will be of special interest to define the earliest point at which abnormal pattern expression can reliably aid in the diagnosis of these disorders.

Expression values for CBDRP were not abnormally elevated in two MSA cohorts. However, while abnormal in the three CBD cohorts that we studied, these values were also elevated in PSP. Expression values for the previously characterized PSPRP (Eckert *et al.*, 2008; Tang *et al.*, 2010*b*) likewise are elevated in independent populations of both CBD and PSP. Moreover, CBDRP and PSPRP expression correlated in individual patients. While CBD and PSP are clinically and pathologically thought to be distinct, both are classified as tauopathies and share deposition of four repeat tau. This contrasts with the mixture of three repeat and four repeat isoforms seen in Alzheimer's disease, suggesting perhaps a shared pathogenesis for the two disorders (Dickson, 1999; Boeve *et al.*, 2003). It is intriguing to speculate that abnormally elevated expression of both patterns in PSP and CBD is also a consequence of regional overlap in their respective neuropathological landscapes. A significant portion of patients with clinical PSP are found to have CBD pathology and vice versa (Josephs *et al.*, 2006; Murray *et al.*, 2007; Ling *et al.*, 2010). Indeed, the correlation between the two patterns, in terms of both spatial topography and subject expression, suggests that the current finding is not simply one of missed diagnoses. Rather, there is true regional overlap between their metabolic profiles.

In addition, despite different pathologies, recent studies have suggested that Alzheimer's disease is a common clinical mimic of CBD (Alexander *et al.*, 2014). Patients with Alzheimer's disease have similar cognitive deficits to CBD, with less rigidity and dystonia (Hu *et al.*, 2009; Hassan *et al.*, 2011). Thus, we performed a preliminary analysis of CBDRP expression in Alzheimer's disease patients, showing that this pattern is not abnormally expressed in these patients relative to healthy controls (personal communication). Indeed, a prior study has demonstrated that the metabolic deficits in Alzheimer's disease tend to involve cortical regions (Habeck *et al.*, 2008) that are rather distinct from those that define the CBDRP topography. Nonetheless, because non-demented subjects exclusively were used to identify and validate the CBDRP topography, it is not clear whether this pattern can effectively differentiate patients with CBD from clinical 'look alike' syndromes with underlying Alzheimer pathology. Further investigation is needed to determine the accuracy of network-based classification in CBD and in clinical mimics of this disorder.

Taking advantage of the clinical asymmetry of CBD, which is a distinctive feature of the disease and its metabolic topography, we measured the degree of hemispheric asymmetry that was present at the network level in the individual subjects. We reasoned that this measure would be more specific in differentiating CBD from the more symmetrical metabolic profile of PSP. Indeed, hemispheric asymmetry for CBDRP expression separated the CBD and PSP groups with greater accuracy than whole-brain CBDRP expression. Ultimately, the classification algorithm based on CBDRP asymmetry index and whole-brain PSPRP expression accurately discriminated between CBD and PSP subjects in whom the precise clinical diagnosis was uncertain at the time they were referred for the imaging study. Classifications of these individuals based upon these imaging measures accorded well with final clinical diagnoses reached independently by movement disorder specialists at clinical follow-up (Tang *et al.*, 2010*b*; Teune *et al.*, 2010; Hellwig *et al.*, 2012). As a result, high specificity and positive predictive value were achieved for image-based classification of CBD on an individual case basis, with all three pathologically confirmed PSP cases classified as non-CBD. These findings provide strong support for the specificity of the CBDRP network and the validity of the classification algorithm that we have identified in this study.

The accuracy of prediction using this automated approach is in line with previously reported values using trained readers (Eckert *et al.*, 2005; Hellwig *et al.*, 2012), but does not require visual judgement whether trained or not. We have previously described an automated algorithm that can differentiate Parkinson's disease from atypical parkinsonian syndromes (excluding CBD), and further subdivide atypical parkinsonian syndromes into MSA and PSP (Tang *et al.*, 2010*b*; Niethammer and Eidelberg, 2012; Tripathi *et al.*, 2012). With the data presented in the present study, we aim to refine this algorithm to include CBD, thereby improving the accuracy of diagnosis in clinically ambiguous cases. We recognize, however, given the protean clinical presentation of CBD, blinded, prospective imaging studies involving larger validation samples and longitudinal network measurements, ideally with post-mortem confirmation, will be necessary to establish the use of CBDRP to assist in diagnosis and for screening potential participants in clinical trials.

Funding

This work was supported in part by the National Institute of Neurological Disorders and Stroke Morris K. Udall Centre of Excellence for Parkinson's Disease Research at The Feinstein Institute for Medical Research (P50 NS071675 to D.E.). The content is solely the responsibility of the authors and does not necessarily represent the official views of the National Institute of Neurological Disorders and Stroke or the National Institutes of Health. The sponsor did not play a role in study design, collection, analysis and interpretation of data, writing of the report or in the decision to submit the paper for publication.

Conflict of interest

Dr Eidelberg serves on the scientific advisory board and has received honoraria from the Michael J. Fox Foundation for Parkinson's Research; is listed as co-inventor of patents re: Markers for use in screening patients for nervous system dysfunction and a method and apparatus for using same, without financial gain; has received research support from the NIH (NINDS, NIDCD, NIAID) and the Dana Foundation; and has served as a consultant

for Pfizer. All other authors declare no competing financial interests.

References

Alexander SK, Rittman T, Xuereb JH, Bak TH, Hodges JR, Rowe JB. Validation of the new consensus criteria for the diagnosis of corticobasal degeneration. J Neurol Neurosurg Psychiatry 2014; 85: 925–9.

Armstrong MJ, Litvan I, Lang AE, Bak TH, Bhatia KP, Borroni B, et al. Criteria for the diagnosis of corticobasal degeneration. Neurology 2013; 80: 496–503.

Boeve BF. The multiple phenotypes of corticobasal syndrome and corticobasal degeneration: implications for further study. J Mol Neurosci 2011; 45: 350–3.

Boeve BF, Lang AE, Litvan I. Corticobasal degeneration and its relationship to progressive supranuclear palsy and frontotemporal dementia. Ann Neurol 2003; 54 (Suppl 5): S15–9.

Boxer AL, Geschwind MD, Belfor N, Gorno-Tempini ML, Schauer GF, Miller BL, et al. Patterns of brain atrophy that differentiate corticobasal degeneration syndrome from progressive supranuclear palsy. Arch Neurol 2006; 63: 81–6.

Burnham KP, Anderson DR. Model selection and multimodel inference. New York: Springer Verlag; 2002.

Dickson DW. Neuropathologic differentiation of progressive supranuclear palsy and corticobasal degeneration. J Neurol 1999; 246 (Suppl 2): II6–15.

Eckert T, Barnes A, Dhawan V, Frucht S, Gordon MF, Feigin AS, et al. FDG PET in the differential diagnosis of parkinsonian disorders. Neuroimage 2005; 26: 912–21.

Eckert T, Tang C, Ma Y, Brown N, Lin T, Frucht S, et al. Abnormal metabolic networks in atypical parkinsonism. Mov Disord 2008; 23: 727–33.

Eidelberg D. Metabolic brain networks in neurodegenerative disorders: a functional imaging approach. Trends Neurosci 2009; 32: 548–57.

Eidelberg D, Dhawan V, Moeller JR, Sidtis JJ, Ginos JZ, Strother SC, et al. The metabolic landscape of cortico-basal ganglionic degeneration: regional asymmetries studied with positron emission tomography. J Neurol Neurosurg Psychiatry 1991; 54: 856–62.

Erbetta A, Mandelli ML, Savoiardo M, Grisoli M, Bizzi A, Soliveri P, et al. Diffusion tensor imaging shows different topographic involvement of the thalamus in progressive supranuclear palsy and corticobasal degeneration. AJNR Am J Neuroradiol 2009; 30: 1482–7.

Fahn S, Oakes D, Shoulson I, Kieburtz K, Rudolph A, Lang A, et al. Levodopa and the progression of Parkinson's disease. N Engl J Med 2004; 351: 2498–508.

Feigin A, Tang C, Ma Y, Mattis P, Zgaljardic D, Guttman M, et al. Thalamic metabolism and symptom onset in preclinical Huntington's disease. Brain 2007; 130: 2858–67.

Habeck C, Foster N, Perneczky R, Kurz A, Alexopoulos P, Koeppe R, et al. Multivariate and univariate neuroimaging biomarkers of Alzheimer's disease. Neuroimage 2008; 40: 1503–15.

Habeck C, Stern Y. Multivariate data analysis for neuroimaging data: overview and application to Alzheimer's disease. Cell Biochem Biophys 2010; 58: 53–67.

Hassan A, Whitwell JL, Josephs KA. The corticobasal syndrome-Alzheimer's disease conundrum. Expert Rev Neurother 2011; 11: 1569–78.

Hellwig S, Amtage F, Kreft A, Buchert R, Winz OH, Vach W, et al. [(1)(8)F]FDG-PET is superior to [(1)(2)(3)I]IBZM-SPECT for the differential diagnosis of parkinsonism. Neurology 2012; 79: 1314–22.

Hu WT, Rippon GW, Boeve BF, Knopman DS, Petersen RC, Parisi JE, et al. Alzheimer's disease and corticobasal degeneration presenting as corticobasal syndrome. Mov Disord 2009; 24: 1375–9.

Huang C, Tang C, Feigin A, Lesser M, Ma Y, Pourfar M, et al. Changes in network activity with the progression of Parkinson's disease. Brain 2007; 130: 1834–46.

Hughes A, Daniel S, Ben-Shlomo Y, Lees A. The accuracy of diagnosis of parkinsonian syndromes in a specialist movement disorder service. Brain 2002; 125: 861–70.

Josephs KA, Petersen RC, Knopman DS, Boeve BF, Whitwell JL, Duffy JR, et al. Clinicopathologic analysis of frontotemporal and corticobasal degenerations and PSP. Neurology 2006; 66: 41–8.

Ling H, O'Sullivan SS, Holton JL, Revesz T, Massey LA, Williams DR, et al. Does corticobasal degeneration exist? A clinicopathological re-evaluation. Brain 2010; 133: 2045–57.

Litvan I. Update on epidemiological aspects of progressive supranuclear palsy. Mov Disord 2003; 18 (Suppl 6): S43–50.

Litvan I, Agid Y, Goetz C, Jankovic J, Wenning GK, Brandel JP, et al. Accuracy of the clinical diagnosis of corticobasal degeneration: a clinicopathologic study. Neurology 1997; 48: 119–25.

Mahapatra RK, Edwards MJ, Schott JM, Bhatia KP. Corticobasal degeneration. Lancet Neurol 2004; 3: 736–43.

Meyer PT, Hellwig S, Amtage F, Rottenburger C, Sahm U, Reuland P, et al. Dual-biomarker imaging of regional cerebral amyloid load and neuronal activity in dementia with PET and 11C-labeled Pittsburgh compound B. J Nucl Med 2011; 52: 393–400.

Murray R, Neumann M, Forman MS, Farmer J, Massimo L, Rice A, et al. Cognitive and motor assessment in autopsy-proven corticobasal degeneration. Neurology 2007; 68: 1274–83.

Niethammer M, Eidelberg D. Metabolic brain networks in translational neurology: concepts and applications. Ann Neurol 2012; 72: 635–47.

Poston K, Tang C, Eckert T, Dhawan V, Frucht S, Vonsattel J, et al. Network correlates of disease severity in multiple system atrophy. Neurology 2012; 78: 1237–44.

Poston KL. Overview of rare movement disorders. Continuum (Minneap Minn) 2010; 16: 49–76.

Sha S, Hou C, Viskontas IV, Miller BL. Are frontotemporal lobar degeneration, progressive supranuclear palsy and corticobasal degeneration distinct diseases? Nat Clin Pract Neurol 2006; 2: 658–65.

Soliveri P, Monza D, Paridi D, Radice D, Grisoli M, Testa D, et al. Cognitive and magnetic resonance imaging aspects of corticobasal degeneration and progressive supranuclear palsy. Neurology 1999; 53: 502–7.

Spetsieris P, Ma Y, Dhawan V, Eidelberg D. Differential diagnosis of parkinsonian syndromes using PCA-based functional imaging features. Neuroimage 2009; 45: 1241–52.

Spetsieris P, Ma Y, Dhawan V, Moeller JR, Eidelberg D. Highly automated computer-aided diagnosis of neurological disorders using functional brain imaging. Proc SPIE Med Imaging 2006; 6144: 61445M1–12.

Spetsieris P, Ma Y, Peng S, Ko JH, Dhawan V, Tang CC, et al. Identification of disease-related spatial covariance patterns using neuroimaging data. J Vis Exp 2013; 76: e50319.

Spetsieris PG, Eidelberg D. Scaled subprofile modeling of resting state imaging data in Parkinson's disease: methodological issues. Neuroimage 2011; 54: 2899–914.

Tang C, Poston K, Dhawan V, Eidelberg D. Abnormalities in metabolic network activity precede the onset of motor symptoms in Parkinson's disease. J Neurosci 2010a; 30: 1049–56.

Tang C, Poston K, Eckert T, Feigin A, Frucht S, Gudesblatt M, et al. Differential diagnosis of parkinsonism: a metabolic imaging study using pattern analysis. Lancet Neurol 2010b; 9: 149–58.

Teune LK, Bartels AL, de Jong BM, Willemsen AT, Eshuis SA, de Vries JJ, et al. Typical cerebral metabolic patterns in neurodegenerative brain diseases. Mov Disord 2010; 25: 2395–404.

Tripathi M, Tang C, Peng S, Dhawan V, Sharma R, Jaimini A, et al. Metabolic image-based algorithm for accurate differential diagnosis of parkinsonism: prospective validation in Indian patient population. J Nucl Med 2012; ; 53 (Suppl 1): 1974.

Vlaar AM, van Kroonenburgh MJ, Kessels AG, Weber WE. Meta-analysis of the literature on diagnostic accuracy of SPECT in parkinsonian syndromes. BMC Neurol 2007; 7: 27.

Zhao P, Zhang B, Gao S. 18F-FDG PET study on the idiopathic Parkinson's disease from several parkinsonian-plus syndromes. Parkinsonism Relat Disord 2012; 18 (Suppl 1): S60–2.